Nonlinear Dyn (2012) 67:2363–2379
DOI 10.1007/s11071-011-0151-y

ORIGINAL PAPER

Chaotic vibrations of a post-buckled L-shaped beam with an axial constraint

Naoki Onozato · Ken-ichi Nagai · Shinichi Maruyama · Takao Yamaguchi

Received: 11 November 2010 / Accepted: 29 June 2011 / Published online: 30 July 2011

Abstract Analytical results are presented on chaotic vibrations of a post-buckled L-shaped beam with an axial constraint. The L-shaped beam is composed of two beams which are a horizontal beam and a vertical beam. The two beams are firmly connected with a right angle at each end. The beams joint with the right angle is attached to a linear spring. The other ends are firmly clamped for displacement. The L-shaped beam is compressed horizontally via the spring at the beams joint. The L-shaped beam deforms to a post-buckled configuration. Boundary conditions are required with geometrical continuity of displacements and dynamical equilibrium with axial force, bending moment, and share force, respectively. In the analysis, the mode shape function proposed by the senior author is introduced. The coefficients of the mode shape function are fixed to satisfy boundary conditions of displacements and linearized equilibrium conditions of force and moment. Assuming responses of the beam with the sum of the mode shape function, then applying the modified Galerkin procedure to the governing equations, a set of nonlinear ordinary differential equations is obtained in a multiple-degree-of-freedom system. Nonlinear responses of the beam are calculated under periodic lateral acceleration. Nonlinear frequency response curves are computed with the harmonic balance method in a wide range of excitation frequency. Chaotic vibrations are obtained with the numerical integration in a specific frequency region. The chaotic responses are investigated with the Fourier spectra, the Poincaré projections, the maximum Lyapunov exponents and the Lyapunov dimension. Applying the procedure of the proper orthogonal decomposition to the chaotic responses, contribution of vibration modes to the chaotic responses is confirmed. The following results have been found: The chaotic responses are generated with the ultra-subharmonic resonant response of the two-third order corresponding to the lowest mode of vibration. The Lyapunov dimension shows that three modes of vibration contribute to the chaotic vibrations predominantly. The results of proper orthogonal decomposition confirm that the three modes contribute to the chaos, which are the first, second, and third modes of vibration. Moreover, the results of the proper orthogonal decomposition are evaluated with velocity which is equivalent to kinetic energy. Higher modes of vibration show larger contribution to the chaotic responses, even though the first mode of vibration has the largest contribution ratio.

N. Onozato · K. Nagai (✉) · S. Maruyama · T. Yamaguchi
Department of Mechanical Engineering, Graduate School of Engineering, Gunma University, 1-5-1 Tenjin-cho, Kiryu, Gunma, 376-8515, Japan
e-mail: kennagai@gunma-u.ac.jp

Keywords Nonlinear vibration · Chaotic vibration · Vibration of continuous system · Beam structure · Analytical procedure · Proper orthogonal decomposition

1 Introduction

Beam-structures are used in transportation products such as aircrafts and vehicles and in measuring fields of micro electronic measuring sensors. The beam-structures are composed with multiple beams, generally. The beam- structures have continuity conditions at each beams joint. It is of practical importance to obtain precise analytical results on nonlinear vibrations of beam-structures.

Nonlinear and chaotic vibrations of a beam have been investigated by many researchers including the authors [1–10]. Pizeshki and Dowell [6] studied chaotic vibrations of a post-buckled beam using the Lyapunov dimension to estimate the number of vibration modes in the chaos. The authors investigated the nonlinear oscillations of a clamped shallow arch [11, 12]. Chaotic vibrations of a post-buckled clamped beam constrained by an axial spring were examined analytically and compared with the experimental results [13]. The results showed that predominant chaotic vibrations of the post-buckled beam bifurcate from subharmonic resonances of one-half and one-third orders. Chaotic vibrations of a clamped-supported beam with a concentrated mass were investigated under several conditions of an axial compression [14]. Chaotic responses of a post-buckled beam with the subharmonic resonances of one-half order and of one-third order were confirmed experimentally. Instability boundaries of the chaos were also examined [15].

On the contrary, there are some researches related to nonlinear vibrations of beam-structures. Wang and Bajaj have studied nonlinear normal modes of a three-beam structure with a tip mass [16]. Modal interaction of a L-shaped beam including torsion and bending were investigated by Warminski et al. [17]. The L-shaped beam had different flexibilities out of plane directions. Internal resonance of a L-shaped beam with a clamped end and free end were studied experimentally and theoretically by Nayfeh et al. [18, 19]. However, it appears to the authors that chaotic vibrations of a post buckled L-shaped beam have not been investigated.

In this paper, chaotic vibrations of a post-buckled L-shaped beam are investigated. Both ends of the L-shaped beam are clamped. The L-shaped beam is constrained by the linear spring for the axial direction along the horizontal beam at the beams joint. Under compression force via the spring, the L-shaped beam has a post-buckled configuration. Moreover, the post-buckled L-shaped beam is subjected to the gravitational acceleration and periodic acceleration. Introducing the mode shape function proposed by the senior author, deflection is assumed as a linear combination of the mode shape function. With the modified Galerkin procedure to the governing equations, a set of nonlinear ordinary differential equations of a multiple degree-of- freedom system is obtained. As fundamental properties of the post buckled L-shaped beam, characteristics of restoring force and the linear natural frequencies are calculated. Then nonlinear periodic vibrations and chaotic vibrations are calculated. Nonlinear frequency response curves of periodic responses are computed with the harmonic balance method. Chaotic responses are computed with the Runge–Kutta method in a specific frequency range. Chaotic responses are inspected with Fourier spectra, Poincaré projection. Using the Lyapunov exponents, chaotic responses are confirmed. The number of vibration modes, contributing to the chaotic vibrations, is examined with the Lyapunov dimension. Utilizing the proper orthogonal decomposition (POD) for the chaotic responses, contribution ratios of vibration modes are examined. The procedure of the POD is applied to the responses of deflection and of velocity. The contribution ratios calculated from the responses of deflection are compared with those from the responses of velocity corresponding to kinetic energy of vibration modes. Furthermore, the kinetic energy is estimated from eigenvalues in calculation of the POD applied to the responses of deflection.

2 Analytical model

The L-shaped beam structure is shown in Fig. 1. The beam structure is constructed with two thin beams, which are a horizontal beam1 with the length L_1 and a vertical beam2 with the length L_2, respectively. The beams have the same dimensions of cross section and material property. The cross section of the L-shaped beam is assumed as a rectangular form of breadth b and of thickness h. The area A is $A = bh$. Symbols ρ, E and I stand for the mass density, the Young's modulus and the moment of inertia of cross section.

Both ends of the beams are connected with right angle with a rigid block. The other ends of the beams are clamped. The symbols M_e and J_e are the mass and the moment of inertia of the rigid block, respectively.

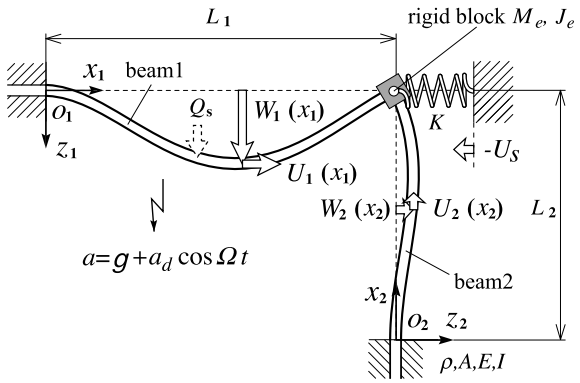

Fig. 1 L-shaped beam constrained by the spring

The beams are constrained by the linear spring with the coefficient K at the beams joint. Coordinate systems of each beam $o_n(x_n, z_n)$, $(n = 1, 2)$ are defined with x_n-axis along the each beam and z_n-axis to the lateral directions of each beam. Suffix n indicates the element number of the L-shaped beam. Suffixes $n = 1$ and $n = 2$ correspond to the horizontal beam1 and the vertical beam2, respectively. Deflection W_n and axial displacement U_n are denoted.

The L-shaped beam is compressed via the spring with the constant displacement of the outer end of the spring $-U_s$. Under the compressional force, the horizontal beam1 is subjected to axial force. The vertical beam2 is also subjected to share force. The L-shaped beam is deformed to a post-buckled configuration. Furthermore, the post-buckled L-shaped beam is subjected to the vertical acceleration $a = g + a_d \cos \Omega t$, where g is the gravitational acceleration and $a_d \cos \Omega t$ is the periodic acceleration. Symbols a_d, Ω and t are the peak amplitude, the excitation angular frequency, and time, respectively. The symbol Q_s is the concentrated force acting on the horizontal beam 1 at the position $\xi_1 = L_s$. The concentrated force Q_s is loaded to calculate characteristics of nonlinear restoring force of the L-shaped beam in the static state of deformation. The concentrated force is removed in the dynamic problem of the beam subjected to periodic acceleration.

3 Problem formulation

The governing equation for nonlinear vibrations of the L-shaped beam is derived with the Hamilton's principle,

$$\delta \int_{t_0}^{t_1} \left(\tilde{T} - \tilde{U} - \tilde{V} + \tilde{f}\right) dt = 0, \tag{1}$$

where $\tilde{T}$, $\tilde{U}$, and $\tilde{V}$ are the kinetic energy, the strain energy, and the potential energy, respectively. The term $\tilde{f}$ represents constraint due to the beams joint of the L-shaped beam.

The kinetic energy $\tilde{T}$ is expressed as follows:

$$\tilde{T} = \sum_{n=1}^{2}\left[\int_0^{L_n} \frac{1}{2}\rho A\left(W_{n,t}^{\,2} + U_{n,t}^{\,2}\right) dx_n\right] + \left[\frac{1}{2}M_e\left(W_{1,t}^{\,2} + U_{1,t}^{\,2}\right) + \frac{1}{2}J_e W_{1,x_1 t}^{\,2}\right]_{x_1 = L_1}, \tag{2}$$

where the first term and the second term correspond to the kinetic energy of both beams and of the rigid block, respectively. The subscripts following a comma stand for partial differentiation.

The strain energy $\tilde{U}$ is given by

$$\tilde{U} = \sum_{n=1}^{2}\left[\int_0^{L_n} \frac{1}{2}EA\left(U_{n,x_n} + \frac{1}{2}W_{n,x_n}^{\,2} - zW_{n,x_n x_n}\right)^2 dx_n\right] + \frac{1}{2}K\{U_s - U_1(L_1)\}^2, \tag{3}$$

where the first term and the second term are the strain energy of the L-shaped beam and of the linear spring, respectively.

The potential energy $\tilde{V}$ generated by the external force becomes

$$\tilde{V} = -\int_0^{L_1} \rho A(g + a_d \cos \Omega t) W_1 \, dx_1 + \int_0^{L_2} \rho A(g + a_d \cos \Omega t) U_2 \, dx_2 - \int_0^{L_1} M_e(g + a_d \cos \Omega t) W_1 \delta(x_1 - L_1) \, dx_1 - \int_0^{L_1} Q_s W_1 \delta(x_1 - L_s) \, dx_1. \tag{4}$$

In the foregoing equation, $\delta(x_1 - L_1)$ is the Dirac's delta function.

The constraint condition is derived from the Lagrange's method of the undetermined multiplier. The constraint condition $\tilde{f}$ at the beams joint is derived as

$$\tilde{f} = \Delta_1[W_1(L_1) + U_2(L_2)] + \Delta_2[U_1(L_1) - W_2(L_2)] + \Delta_3[W_{1,x_1}(L_1) - W_{2,x_2}(L_2)], \tag{5}$$

where symbols Δ_1, Δ_2, and Δ_3 are undetermined multipliers. Continuity conditions at the beams joint are given by

$$W_1(L_1) + U_2(L_2) = 0, \tag{6}$$

$$U_1(L_1) - W_2(L_2) = 0, \tag{7}$$

$$W_{1,x_1}(L_1) - W_{2,x_2}(L_2) = 0. \tag{8}$$

Equations (6) to (8) correspond to the condition of the continuity between the deflection of one beam and the axial displacement of the other beam and the condition between the rotations of the two beams.

Consequently, the governing equation of nonlinear vibrations of the L-shaped beam is obtained as

$$\begin{aligned}
&-\int_{t_0}^{t_1}\Bigg[\int_0^{L_1}\{\rho A W_{1,tt} - (N_{x_1}W_{1,x_1})_{,x_1} \\
&\quad + EIW_{1,x_1x_1} - \rho A(g + a_d\cos\Omega t) \\
&\quad - Q_s\delta(x_1 - L_s)\}\delta W_1\,dx_1 \\
&\quad + \int_0^{L_1}\{\rho A U_{1,tt} - N_{x_1,x_1}\}\delta U_1\,dx_1 \\
&\quad + \int_0^{L_2}\{\rho A W_{2,tt} - (N_{x_2}W_{2,x_2})_{,x_2} \\
&\quad + EIW_{2,x_2x_2}\}\delta W_2\,dx_2 \\
&\quad + \int_0^{L_2}\{\rho A U_{2,tt} - N_{x_2,x_2} \\
&\quad + \rho A(g + a_d\cos\Omega t)\}\delta U_2\,dx_2 \\
&\quad + B(W_1, U_1, W_2, U_2)\Bigg]dt = 0,
\end{aligned} \tag{9}$$

where the axial force N_{x_n} of the beams is expressed as $N_{x_n} = EA\{U_{n,x_n} + (1/2)\,W_{n,x_n}^2\}$, $(n = 1, 2)$. The formulation $B(W_1, U_1, W_2, U_2)$ corresponds to dynamical and geometrical condition at the boundaries of the two beams. Details of the formulation are expressed as follows:

$$\begin{aligned}
&B(W_1, U_1, W_2, U_2) \\
&= [(M_e W_{1,tt} + N_{x_1}W_{1,x_1} - EIW_{1,x_1x_1x_1} \\
&\quad - M_e(g + a_d\cos\Omega t) - \Delta_1)\delta W_1]_{x_1=L_1} \\
&\quad + [(M_e U_{1,tt} + N_{x_1} - \Delta_2)\delta U_1]_{x_1=L_1} \\
&\quad + [(J_e W_{1,x_1tt} + EIW_{1,x_1x_1} - \Delta_3)\delta W_{1,x_1}]_{x_1=L_1} \\
&\quad + [(N_{x_2}W_{2,x_2} - EIW_{2,x_2x_2x_2} + \Delta_2)\delta W_2]_{x_2=L_2} \\
&\quad + [(N_{x_2} - \Delta_1)\delta U_2]_{x_2=L_2} \\
&\quad + [(EIW_{2,x_2x_2} + \Delta_3)\delta W_{2,x_2}]_{x_2=L_2} \\
&\quad - \{W_1(L_1) - U_2(L_2)\}\delta\Delta_1 \\
&\quad - \{U_1(L_1) - W_2(L_2)\}\delta\Delta_2 \\
&\quad - \{W_{1,x_1}(L_1) - W_{,x_1}(L_2)\}\delta\Delta_3 \\
&\quad - [(N_{x_1}W_{1,x_1} - EIW_{1,x_1x_1x_1})\delta W_1]_{x_1=0} \\
&\quad - [(N_{x_2}W_{2,x_2} - EIW_{2,x_2x_2x_2})\delta W_2]_{x_2=0} \\
&\quad - [(N_{x_1})\delta U_1]_{x_1=0} \\
&\quad - [(N_{x_2})\delta U_2]_{x_2=0} \\
&\quad - [(EIW_{1,x_1x_1})\delta W_{1,x_1}]_{x_1=0} \\
&\quad - [(EIW_{2,x_2x_2})\delta W_{2,x_2}]_{x_2=0}.
\end{aligned} \tag{10}$$

In the foregoing equation, each term is required to be zero, then the undetermined multipliers are given by the following equations:

$$\Delta_1 = [N_{x_2}]_{x_2=L_2}, \tag{11}$$

$$\Delta_2 = -[N_{x_2}W_{2,x_2} - EIW_{2,x_2x_2x_2}]_{x_2=L_2}, \tag{12}$$

$$\Delta_3 = -[EIW_{2,x_2x_2}]_{x_2=L_2}. \tag{13}$$

Substituting (11) to (13) into (10), the governing equation without the undetermined multipliers is obtained.

The nondimensional quantities are introduced as follows:

$$\begin{aligned}
&w_n = \frac{W_n}{r}, \quad u_n = \frac{U_n L_n}{r^2}, \quad u_s = \frac{U_s L_1}{r^2}, \quad \xi_n = \frac{x_n}{L_n}, \\
&\Gamma_1 = \frac{r}{L_1}, \quad \tau = \Omega_0 t, \quad \omega = \frac{\Omega}{\Omega_0}, \quad \beta_e = \frac{M_e}{\rho A L_1}, \\
&\gamma_e = \frac{J_e}{\rho A L_1}, \quad k = \frac{KL_1}{EA}, \quad n_{x_n} = \frac{N_{x_n}L_n^2}{EI}, \\
&n_c = \frac{n_{x_1}}{n_{cr}}, \quad q_s = \frac{Q_s L_1^3}{EIr}, \quad [p_s, p_d] = [g, a_d]\frac{\rho A L_1^4}{EIr}, \\
&l = \frac{L_2}{L_1}, \quad l_s = \frac{L_s}{L_1}, \quad (n = 1,\ 2),
\end{aligned} \tag{14}$$

where $r = \sqrt{I/A}$ and $\Omega_0 = (1/L_1^2)\sqrt{EI/(\rho A)}$. The symbol r is the radius of gyration of the cross section of the beam. The symbol Ω_0 represents the coefficient of the lowest natural frequency of the beam1. The symbol w_n is the nondimensional deflection normalized by the radius of gyration r. The symbols u_n and u_s are the nondimensional axial displacement of the two beams and the nondimensional displacement of the outer end of the spring, respectively. The symbol ξ_n is the nondimensional coordinate. The symbol Γ_1 is the slenderness ratio. The symbol τ is the nondimensional time. The symbol ω is the nondimensional frequency. The symbols β_e and γ_e are the nondimensional mass and the nondimensional moment of inertia of the rigid block. The symbol k is the nondimensional spring constant. The symbol n_{x_n} is the nondimensional axial force of the two beams. The symbol n_c is the compression ratio of the axial force n_{x_1} to the buckling load n_{cr}. The symbol q_s is the nondimensional load. The symbols p_s and p_d are the nondimensional acceleration related to the gravity and the nondimensional intensity of the periodic acceleration, respectively. The symbol l is the ratio of the length of the vertical beam2 to that of the horizontal beam1. The symbol l_s is the nondimensional concentrated loading position.

Assuming the dynamic problem of the thin beam with lower bending vibration, effects of axial inertia, rotating inertia, and shear deformation on the beam can be neglected. At the beams joint of the L-shaped beam, the rotation due to the bending deformation is larger than the axial displacement, generally. Thus, the rotating inertia of the rigid block at the beams joint is included in the governing equation. The axial inertia of the block can be neglected in the analysis. The nondimensional governing equations of the nonlinear vibrations of the L-shaped beam are shown as follows:

$$
\begin{aligned}
&-\int_{t_0}^{t_1}\Bigg[\int_0^1 \{w_{1,\tau\tau} - (n_{x_1} w_{1,\xi_1})_{,\xi_1} + w_{1,\xi_1\xi_1\xi_1\xi_1} \\
&\quad - (p_s + p_d\cos\omega\tau) - \delta(\xi_1 - l_s) q_s\}\delta w_1\, d\xi_1 \\
&\quad + \int_0^1 \Bigg\{ l w_{2,\tau\tau} - \frac{1}{l^3}(n_{x_2} w_{2,\xi_2})_{,\xi_2} \\
&\quad + \frac{1}{l^3} w_{2,\xi_2\xi_2\xi_2\xi_2} \Bigg\}\delta w_2\, d\xi_2 \\
&\quad + b(w_1, u_1, w_2, u_2)\Bigg] d\tau = 0, \qquad (15)
\end{aligned}
$$

$b(w_1, u_1, w_2, u_2)$

$$
\begin{aligned}
&= +\Bigg[\Bigg\{ n_{x_1} w_{1,\xi_1} - w_{1,\xi_1\xi_1\xi_1} - \beta_e(p_s + p_d\cos\omega\tau) \\
&\quad - \frac{1}{\Gamma_1 l^2} n_{x_2}(1)\Bigg\}\delta w_1\Bigg]_{\xi_1=1} \\
&\quad + \Bigg[\Bigg\{ n_{x_1} + \frac{\Gamma_1}{l^3}(n_{x_2}(1) w_{2,\xi_2}(1) - w_{2,\xi_2\xi_2\xi_2}(1)) \\
&\quad - k(u_s - u_1)\Bigg\}\delta u_1\Bigg]_{\xi_1=1} \\
&\quad + \Bigg[\Bigg\{ \gamma_e w_{1,\xi_1\tau\tau} + w_{1,\xi_1\xi_1} \\
&\quad + \frac{1}{l^2} w_{2,\xi_2\xi_2}(1)\Bigg\}\delta w_{1,\xi_1}\Bigg]_{\xi_1=1} \\
&\quad - \Bigg[\frac{1}{l^2}\Bigg\{\frac{l}{\Gamma_1} w_1(1) + u_2(1)\Bigg\}\delta n_{x_2}\Bigg]_{\xi_2=1} \\
&\quad + \Bigg[\frac{1}{l^3}\Bigg\{\Gamma_1 u_1(1) + w_2(1)\Bigg\}\delta(n_{x_2} w_{2,\xi_2})\Bigg]_{\xi_2=1} \\
&\quad + \Bigg[\frac{1}{l^3}\{\Gamma_1 u_1(1) + w_2(1)\}\delta(-w_{2,\xi_2\xi_2\xi_2})\Bigg]_{\xi_2=1} \\
&\quad + \Bigg[\frac{1}{l^2}\Bigg\{ w_{1,\xi_2}(1) + \frac{1}{l} w_{2,\xi_2}(1)\Bigg\}\delta w_{2,\xi_2\xi_2}\Bigg]_{\xi_2=1} \\
&\quad - [\{n_{x_1} w_{1,\xi_1} - w_{1,\xi_1\xi_1\xi_1}\}\delta w_1]_{\xi_1=0} \\
&\quad - \Bigg[\frac{1}{l^3}(n_{x_2} w_{2,\xi_2} - w_{2,\xi_2\xi_2\xi_2})\delta w_2\Bigg]_{\xi_2=0} \\
&\quad - [n_{x_1}\delta u_1]_{\xi_1=0} - \Bigg[\frac{1}{l^3} n_{x_2}\delta u_2\Bigg]_{\xi_2=0} \\
&\quad - [(w_{1,\xi_1\xi_1})\delta w_{1,\xi_1}]_{\xi_1=0} \\
&\quad - \Bigg[\frac{1}{l^3}(w_{2,\xi_2\xi_2})\delta w_{2,\xi_2}\Bigg]_{\xi_2=0}. \qquad (16)
\end{aligned}
$$

The axial force n_{x_n} $(n = 1, 2)$ acting on the cross section of the beams is derived from the first and second terms in the above equation as follows:

$$
\begin{aligned}
n_{x_1} &= \frac{k}{1+k}\Bigg\{ u_s + \int_0^1 (1/2) w_{1,\xi_1}^2\, d\xi_1\Bigg\} \\
&\quad + \frac{1}{1+k}\Bigg[\frac{\Gamma_1^2}{l}\{w_{1,\xi_1\xi_1\xi_1}(1) \\
&\quad + \beta_e(p_s + p_d\cos\omega\tau)\} w_{2,\xi_2}(1)\Bigg]
\end{aligned}
$$

$$+\frac{1}{1+k}\left[\frac{\Gamma_1}{l^3}w_{2,\xi_2\xi_2\xi_2}(1)\right], \tag{17}$$

$$\begin{aligned} n_{x_2} = {} & \frac{k}{1+k}\left(\Gamma_1 l^2\right)\left\{u_s + \int_0^1 (1/2)w_{1,\xi_1}^2\, d\xi_1\right\}w_{1,\xi_1}(1) \\ & -\left(\Gamma_1 l^2\right)\{w_{1,\xi_1\xi_1\xi_1}(1) + \beta_e(p_s + p_d\cos\omega\tau)\} \\ & +\frac{1}{1+k}\left[\frac{\Gamma_1^2}{l}w_{2,\xi_2\xi_2\xi_2}(1)w_{1,\xi_1}(1)\right] \\ & +\frac{\Gamma_1}{l}(p_s + p_d\cos\omega\tau)(\xi_2 - 1), \end{aligned} \tag{18}$$

where the term $\Gamma_1^2 w_{1,\xi_1}^2$ at the position $\xi_1 = 1$, which appears in the derivation of the above equations, is small compared with the term $1+k$. The term $\Gamma_1^2 w_{1,\xi_1}^2$ is neglected. The displacement of the beams at the beams joint $u_n(1)$ $(n = 1, 2)$ is given by the following equations:

$$u_1(1) = n_{x_1} - \int_0^1 \frac{1}{2}w_{1,\xi_1}^2\, d\xi_1, \tag{19}$$

$$u_2(1) = n_{x_2} - \int_0^1 \frac{1}{2}w_{2,\xi_2}^2\, d\xi_2 - \frac{\Gamma_1}{2l}(p_s + p_d\cos\omega\tau). \tag{20}$$

The boundary conditions for deflection w_n $(n = 1, 2)$ and for displacement u_n $(n = 1, 2)$ and the continuity conditions at the beams joint are given as:

$$\begin{aligned} & \xi_1 = 0; \quad u_1 = 0,\ w_1 = 0,\ w_{1,\xi_1} = 0, \\ & \xi_2 = 0; \quad u_2 = 0,\ w_2 = 0,\ w_{2,\xi_2} = 0, \\ & \xi_1 = \xi_2 = 1; \\ & w_1 + \frac{\Gamma_1}{l}u_2 = 0, \\ & \Gamma_1 u_1 - w_2 = 0, \\ & w_{1,\xi_1} - \frac{1}{l}w_{2,\xi_2} = 0, \\ & n_{x_1}w_{1,\xi_1} - w_{1,\xi_1\xi_1\xi_1} - \beta_e(p_s + p_d\cos\omega\tau) \\ & \quad - \frac{1}{\Gamma_1 l^2}n_{x_2} = 0, \\ & n_{x_1} + \Gamma_1 l^3(n_{x2}w_{2,\xi_2} - w_{2,\xi_2\xi_2\xi_2}) - k(u_s - u_1) = 0, \\ & \gamma_e w_{1,\xi_1\tau\tau} + w_{1,\xi_1\xi_1} + \frac{1}{l^2}w_{2,\xi_2\xi_2} = 0. \end{aligned} \tag{21}$$

In (21), the continuity conditions at the beams joint include nonlinear terms $n_{x_1}w_{1,\xi_1}$ and $n_{x_2}w_{2,\xi_2}$. Therefore, the analysis of the L-shaped beam including the nonlinear continuity condition is conducted as shown in the next section.

4 Analytical procedure

4.1 Reduction to a multiple degree-of-freedom system

Applying the modified Galerkin procedure to the governing equations including the nonlinear continuity conditions, a set of nonlinear differential equations is obtained with a multiple degree-of-freedom system. First, the static deformation is calculated in a post-buckled state. Next, natural modes of vibration are calculated under the post-buckled configuration. Based on the vibration modes, the standard form of nonlinear ordinary differential equations is obtained in the post-buckled state.

The deflection w_n of each beam is assumed as:

$$\begin{aligned} & w_n(\xi_n, \tau) = \sum_j b_j(\tau)\zeta_{nj}(\xi_n), \\ & \zeta_{nj}(\xi_n) \\ & \quad = \sum_{k=1}^{5} c_{njk}\xi_n^{k-1}(\cos p_{1nj}\pi\xi_n + q_{nj}\sin p_{2nj}\pi\xi_n), \\ & \quad (n = 1, 2,\ \ j = 1, 2, 3, \ldots), \end{aligned} \tag{22}$$

where $b_j(\tau)$ is the unknown time function. The mode shape function $\zeta_{nj}(\xi_n)$ is proposed by the senior author [20, 21].

The mode shape function includes static deformation and is suitable to vibration modes of the L-shaped beam. The mode shape function is expressed as the product of the truncated power series and the trigonometric function. The truncated power series function expresses static deformation of the L-shaped beam. The trigonometric function enables the deflection w_n to predict higher modes of vibration. By choosing the coefficients c_{njk}, the mode shape function satisfies the geometrical boundary conditions and linearized continuity conditions within a relatively small deflection in a pre-buckled state. The coefficients c_{njk} of the truncated power series function and the coefficients p_{1nj},

p_{2nj} and q_{nj} of the trigonometric function are listed in Appendix A.

Substituting (22) into the governing equation (15) and applying the modified Galerkin procedure, a set of nonlinear ordinary differential equation is derived as follows:

$$\sum_j \hat{B}_{ij} b_{j,\tau\tau} + \sum_j \{\hat{C}_{ij} + \hat{R}_{ij}(p_s + p_d \cos\omega\tau)\} b_j + \sum_j \sum_k \{\hat{D}_{ijk} + \hat{R}'_{ijk}(p_s + p_d \cos\omega\tau)\} b_j b_k + \sum_j \sum_k \sum_l \hat{E}_{ijkl} b_j b_k b_l - \hat{F}_i - (p_s + p_d \cos\omega\tau)\hat{G}_i - q_s \hat{H}_i = 0 \quad (i, j, k, l = 1, 2, 3, \ldots), \tag{23}$$

where the notations are listed in Appendix B.

To find the deflection of the post-buckled L-shaped beam under the static force, the terms of inertia force and the periodic force are neglected. The unknown time coefficient $b_j(\tau)$ is replaced by the unknown constant coefficient $\bar{b}_j$ in (22). With the substitution of $\bar{b}_j$ into (23), simultaneous cubic equations for the static deflection are given by

$$\sum_j (\hat{C}_{ij} + \hat{R}_{ij} p_s)\bar{b}_j + \sum_j \sum_k (\hat{D}_{ijk} + \hat{R}'_{ijk} p_s)\bar{b}_j \bar{b}_k + \sum_j \sum_k \sum_l \hat{E}_{ijkl} \bar{b}_j \bar{b}_k \bar{b}_l - \hat{F}_i - p_s \hat{G}_i - q_s \hat{H}_i = 0. \tag{24}$$

The coordinate $\tilde{b}_j(\tau)$ for deflection is introduced to calculate dynamic responses of the L-shaped beam. The coordinate $\tilde{b}_j(\tau)$ represents unknown time function of the dynamic deflection from the static equilibrium position in the post-buckled state. Substituting $b_j(\tau) = \bar{b}_j + \tilde{b}_j(\tau)$ into (23), the nonlinear equations with $\bar{b}_j$ and $\tilde{b}_j(\tau)$ are obtained as

$$\sum_j \hat{B}_{ij} \tilde{b}_{j,\tau\tau} + \sum_j (\tilde{C}_{ij} + \tilde{P}_{ij} p_d \cos\omega\tau)\tilde{b}_j + \sum_j \sum_k (\tilde{D}_{ijk} + \tilde{P}'_{ijk} p_d \cos\omega\tau)\tilde{b}_j \tilde{b}_k + \sum_j \sum_k \sum_l \hat{E}_{ijkl} \tilde{b}_j \tilde{b}_k \tilde{b}_l - \hat{G}_i p_d \cos\omega\tau = 0, \tag{25}$$

where

$$\begin{aligned}
\tilde{C}_{ij} &= \hat{C}_{ij} + \sum_k (\hat{D}_{ijk} + \hat{D}_{ikj})\bar{b}_k + \sum_k \sum_l (\hat{E}_{ijkl} + \hat{E}_{iklj} + \hat{E}_{iljk})\bar{b}_k \bar{b}_l, \\
\tilde{P}_{ij} &= \hat{R}_{ij} + \sum_k (\hat{R}'_{ijk} + \hat{R}'_{ikj})\bar{b}_k, \\
\tilde{D}_{ijk} &= \hat{D}_{ijk} + \sum_l (\hat{E}_{ijkl} + \hat{E}_{iklj} + \hat{E}_{iljk})\bar{b}_l, \\
\tilde{P}'_{ijk} &= \hat{R}'_{ijk}.
\end{aligned} \tag{26}$$

Omitting the nonlinear terms and the periodic force, a set of homogeneous linear equations is obtained for free vibration. Both the natural frequencies ω_i of the ith mode and the corresponding eigenvectors ϕ_{iq} are calculated. The linear natural mode of vibration $\tilde{\zeta}_{ni}$ is expressed with ϕ_{iq} as follows:

$$\tilde{\zeta}_{ni}(\xi_n) = \frac{1}{n_i} \sum_q \psi_{qi} \zeta_{nq}, \quad \psi_{qi} = \frac{\phi_{iq}}{\sqrt{\sum_k \sum_l \phi_{ik} \hat{B}_{kl} \phi_{il}}} \quad (n = 1, 2; q, k, l = 1, 2, 3, \ldots), \tag{27}$$

where the symbol n_i denotes arbitrary constants to normalize the maximum amplitude of each vibration mode to unity.

The equation with the variable $\tilde{b}_j$ is transformed to a standard form of nonlinear ordinary differential equations to obtain dynamic responses. Denoting $\tilde{b}_i^{(1)}(\tau)$ as the normal coordinates corresponding to $\tilde{\zeta}_{ni}$, the dynamic deflection $w_n(\xi_n, \tau)$ from the static equilibrium position is assumed as:

$$w_n(\xi_n, \tau) = \sum_i b_i^{(1)}(\tau)\tilde{\zeta}_{ni}(\xi_n) \quad (n = 1, 2,\ i = 1, 2, 3, \ldots). \tag{28}$$

Transforming the equation of the variable $\tilde{b}_j(\tau)$ to the normal coordinates $b_i^{(p)}(\tau)$, $(p = 1, 2)$, one can obtain a set of nonlinear differential equations in the state

space of $b_i^{(p)}(\tau)$ as

$$
\begin{aligned}
&b_i^{(1)},_\tau = b_i^{(2)},\\
&b_i^{(2)},_\tau = -2\varepsilon_i\omega_i b_i^{(2)} - \omega_i^2 b_i^{(1)} - \sum_j P_{ij}\, p_d \cos\omega\tau\, b_j^{(1)}\\
&\qquad - \sum_j \sum_k (D_{ijk} + P'_{ijk}\, p_d \cos\omega\tau) b_j^{(1)} b_k^{(1)}\\
&\qquad - \sum_j \sum_k \sum_l E_{ijkl} b_j^{(1)} b_k^{(1)} b_l^{(1)} + G_i\, p_d \cos\omega\tau,
\end{aligned}
\tag{29}
$$

where

$$
\begin{aligned}
P_{ij} &= \frac{n_i}{n_j} \sum_p \sum_q \tilde{P}_{pq} \psi_{pi} \psi_{qj},\\
D_{ijk} &= \frac{n_i}{n_j n_k} \sum_p \sum_q \sum_q \tilde{D}_{pqr} \psi_{pi} \psi_{qj} \psi_{rk},\\
P'_{ijk} &= \frac{n_i}{n_j n_k} \sum_p \sum_q \sum_r \tilde{P}'_{pqr} \psi_{pi} \psi_{qj} \psi_{rk},\\
E_{ijkl} &= \frac{n_i}{n_j n_k n_l} \sum_p \sum_q \sum_r \sum_s \tilde{E}_{pqrs} \psi_{pi} \psi_{qj} \psi_{rk} \psi_{sl},\\
G_i &= n_i \sum_p \hat{G}_i \psi_{pi}, \qquad (p, q, r, s = 1, 2, 3, \cdots).
\end{aligned}
\tag{30}
$$

In (29), $b_i^{(1)}(\tau)$ and $b_i^{(2)}(\tau)$ correspond to the deflection and the velocity in the state space, respectively. New dissipation terms of linear damping are introduced. The symbol ε_i represents damping ratio corresponding to the ith mode of vibration. After the transformation to the standard form of (29), the nonlinear dynamic responses of the post-buckled L-shaped beam are calculated with the reduced number of modes I_c.

4.2 Periodic responses and chaotic responses

Frequency response curves of periodic vibrations are obtained with the harmonic balance method. Periodic responses are assumed as

$$
\begin{aligned}
b_i^{(1)}(\tau) &= C_{i1\mu 0}\\
&\quad + \sum_p [C_{i1\mu p} \cos\mu p\omega\tau + C_{i2\mu p} \sin\mu p\omega\tau]\\
&\quad (i = 1, 2, 3, \ldots, I_c;\ p = 1, 2, 3, \ldots),
\end{aligned}
\tag{31}
$$

where $C_{i1\mu 0}$ and $C_{ij\mu p}$ $(j = 1, 2;\ p = 1, 2, 3, \ldots)$ are unknown constants. To calculate the principal resonance, subharmonic resonance and ultra-subharmonic resonance, μ is chosen as unity. Amplitude of the response is expressed as a root mean square value $\tilde{w}_{n\mathrm{rms}}$.

Chaotic responses are calculated with the Runge–Kutta method.

4.3 Lyapunov components and Lyapunov dimension

The Lyapunov exponents are calculated with the procedure by Wolf et al. [22] and Shimada et al. [23] to confirm whether response is the chaos. If the Lyapunov exponents have one or more positive values, the response is confirmed as the chaotic vibration. Using the Lyapunov exponents, the Lyapunov dimension d_L is also calculated [24] increasing the assumed number of modes I_c. When d_L converges to a constant value, one can estimate the number of vibration modes which contribute to the chaos [6].

4.4 Proper orthogonal decomposition

The proper orthogonal decomposition (POD), which is also called as Karhunen–Loève transformation [25–28], is applied to chaotic responses of the post-buckled L-shaped beam. The POD enables to clarify the modal patterns in the chaotic responses and their contribution ratios. The modal patterns correspond to modes of vibration. In the POD, the covariance matrix of the simultaneous time responses at the multiple positions ξ_{np} $(p = 1, 2, 3, \ldots, d)$ is calculated.The covariance matrix is transformed to an orthogonal matrix, which results in the eigenvalue problem of the covariance matrix. The eigenvalue p_i corresponds to the contribution of model pattern represented by the eigenvector $\boldsymbol{\Phi}$. Contribution ratio μ_i of the ith modal pattern to the all modal patterns is calculated as

$$
\mu_i = \frac{p_i}{\sum_{j=1}^{d} p_j}. \tag{32}
$$

5 Results and discussion

The L-shaped beam is deformed to the post-buckled configuration under the axial compressive force with the spring. First, the fundamental properties of the post-buckled L-shaped beam are inspected. Next, dynamic responses of the L-shaped beam are investigated

Table 1 Parameter list

Spring coefficient	$k = 0.03$
Length ratio	$l = 0.707$
Mass ratio of the rigid block	$\beta_e = 1.57$
Moment of inertia of the rigid block	$\gamma_e = 4.9 \times 10^{-4}$
Compression ratio	$n_c = 1.014$
Damping ratio	$\epsilon_i = 0.01$
Maximum number of vibration modes	$I_c = 5$

with the harmonic balance method and the numerical integration. Table 1 shows the representative parameters used in the analysis. The post-buckled L-shaped beam satisfies the one to two internal resonant condition between the first mode and the second mode. The internal resonant condition is also obtained in the beam without the axial compression by the spring.

5.1 Fundamental properties of the L-shaped beam

The deformed shapes of the L-shaped beam under the gravity and the axial compression are shown in Fig. 2(a) and (b). The figures (a) and (b) correspond to the deformed shapes of the horizontal beam and of the vertical beam, respectively. The deformed shapes are shown under the compression ratio $n_c = 0$ and $n_c = 1.014$. The L-shaped beam without axial compression $n_c = 0$ shows the maximum deflection $\bar{w}_1 = 0.16$ at the position $\xi_1 = 0.55$. Under the compression ratio $n_c = 1.014$, the deformed shape of the beam increases to the deflection $\bar{w}_1 = 3.7$ at the same position. Figure 3 shows the characteristics of restoring force of the L-shaped beam under concentrated force q_s. The concentrated force is loaded on the center of the horizontal beam. The deflection of the horizontal beam $\bar{w}_1$ is observed at the position $\xi_1 = 0.5$. The characteristics of restoring force show the type of a hardening spring dominantly under the compression ratio $n_c = 0$. The characteristics of the type of a hardening spring are caused because of the share force of the vertical beam and the axial force of the spring. In contrast, the characteristics of restoring force of the post-buckled beam under the compression ratio $n_c = 1.014$ show the type of a softening-and-hardening spring with negative gradient. The characteristics of the type of a softening-and-hardening spring are caused by the axial compression.

The natural frequencies ω_i, $(i = 1, \ldots, 5)$ and the natural modes of vibration are shown in Table 2, where

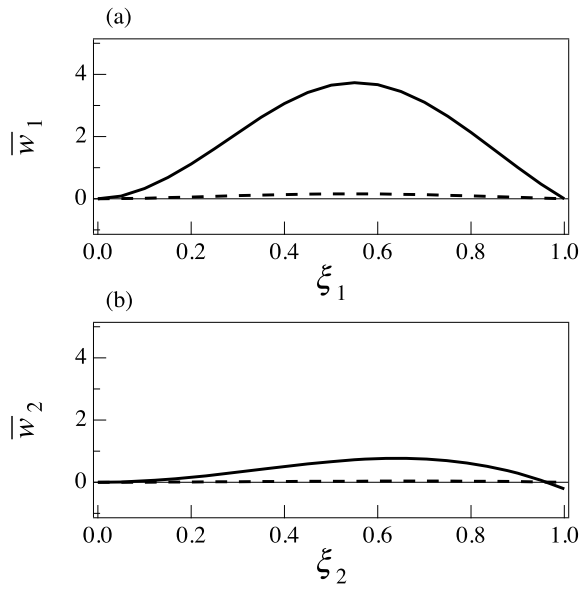

Fig. 2 Deformed configuration of the L-shaped beam subjected to the gravitational force, – – –: under the compression ratio $n_c = 0$; ——: under the compression ratio $n_c = 1.014$

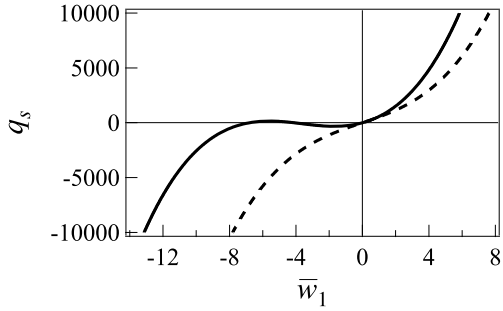

Fig. 3 Characteristics of restoring force of the L-shaped beam subjected to the concentrated force and the gravitational force, – – –: under the compression ratio $n_c = 0$; ——: under the compression ratio $n_c = 1.014$

the symbol i indicates the order of vibration modes. Natural frequencies of the first and second modes of vibration satisfy the condition of the internal resonance $2\omega_1 \approx \omega_2$.

5.2 Nonlinear frequency response curves of the L-shaped beam

Nonlinear frequency-response curves of the post-buckled beam in the case of $n_c = 1.014$ are calculated under the gravitational force $p_s = 146$ and under the periodic excitation force $p_d \cos \omega\tau$. The amplitude

Table 2 Natural frequencies and natural modes of vibration of the L-shaped beam,– – –: under the axial compression ratio $n_c = 0$, ——: under the axial compression ratio $n_c = 1.014$

i	1	2	3
$\omega_i\,(n_c = 0)$	18.1	36.6	57.0
$\omega_i\,(n_c = 1.014)$	16.5	32.6	46.3
Natural mode of vibration	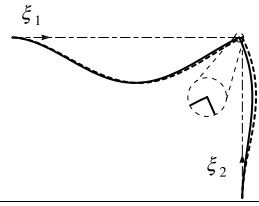	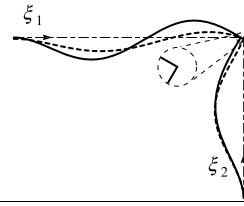	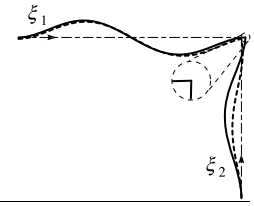
i	4	5	
$\omega_i\,(n_c = 0)$	99.4	123	
$\omega_i\,(n_c = 1.014)$	89.6	116	
Natural mode of vibration	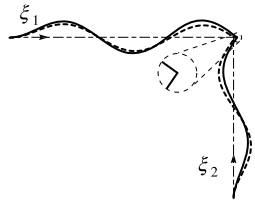	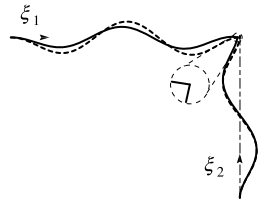	

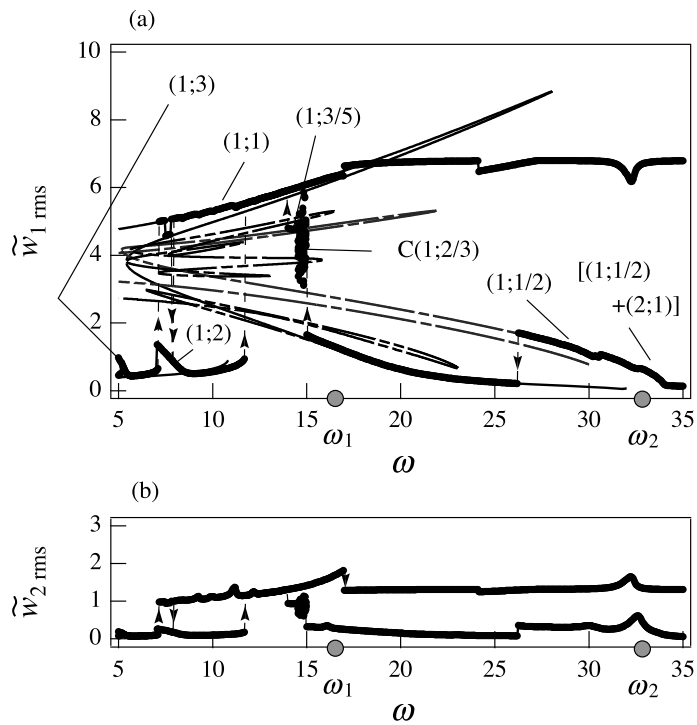

Fig. 4 Frequency response curves of the L-shaped beam under the gravitational force $p_s = 146$; •: the results of numerical integration; ——— : (1;1); — – —: (1;1/2); — – – —: (1;2/3); (**a**) the response of the horizontal beam; (**b**) the response of the vertical beam

of the periodic excitation force p_d is kept constant $p_d = 365$. The excitation frequency ω is swept from $\omega = 5$ to $\omega = 35$. Figures 4(a) and (b) show the frequency response curves of the horizontal beam and of the vertical beam, respectively. The ordinate indicates the nondimensional amplitude $\tilde{w}_{i\mathrm{rms}}$ $(i = 1, 2)$

of the response $\tilde{w}_i$ with a root mean square value at the center of each beam. The abscissa indicates the nondimensional excitation frequency. Thin lines indicate periodic responses obtained with harmonic balance method, while thick lines indicate the results by the numerical integration. The solid circles on the abscissa indicate the natural frequencies of the L-shaped beam. The notation $(i; j)$ indicates the type of nonlinear resonance with jth order accompanied with the vibration mode of ith order. The chaotic response is shown by the notation C$(i; j)$, where the index $(i; j)$ means the predominant mode of vibration and the predominant type of nonlinear resonance of jth order in the chaotic response as shown below.

When the excitation frequency increases from $\omega =$ 5, the response of the super harmonic resonance (1;3) with the lowest mode is generated. At the excitation frequency $\omega = 7.2$, the nonresonant response with the lowest mode jumps to the principal resonance (1;1). The principal resonance shows the type of a hardening spring. When the excitation frequency increases to $\omega = 7.8$, the response jumps to the curve of the super-harmonic resonance (1;2) of the second order, which has the type of a softening spring. At the excitation frequency $\omega = 11.8$, the periodic response of the principal resonance (1;1) are generated again. At the frequency $\omega = 17$, the periodic response jumps to the curve of the response around the static equilibrium position of deflection $\bar{w}_1 = -6.8$ as shown in Fig. 3.

When the excitation frequency decreases from $\omega =$ 35 to the second natural frequency ω_2, the internal resonant response [(1;1/2)+(2;1)] is generated accompanied with the lowest mode and the second mode of vibration. At the excitation frequency $\omega = 30$, the sub-harmonic resonance (1;1/2) of one-second order shows the type of a softening spring. The response (1;1/2) jumps to the nonresonant response at the frequency $\omega = 26.2$. Amplitude of the principal resonant response (1;1) with the type of a softening spring increases from near $\omega = 20$. When the excitation frequency decreases from $\omega = 15.0$, nonperiodic responses are generated. The responses are confirmed as the chaos. Detailed inspection of the chaotic responses are discussed as following sections.

The chaotic responses C(1;2/3) are generated with the ultra-subharmonic resonance (1;2/3) predominantly including the subharmonic resonance (1;1/2) and the ultra-subharmonic resonance (1;3/5). The chaotic responses are generated from $\omega = 15.0$ to $\omega = 14.6$. The chaotic responses change to the periodic response of the ultra-subharmonic resonance (1;3/5) at the frequency $\omega = 14.5$. The principal resonant response is generated in the frequency region from $\omega = 14$ to $\omega = 7.9$. Furthermore, the principal resonant response jumps to the response of the superharmonic resonance (1;2) at the frequency $\omega = 7.9$.

5.3 Time histories, Fourier spectra, and Poincaré projections of the chaotic responses

The chaotic responses C(1;2/3) of the L-shaped beam are generated under the excitation amplitude $p_d =$ 365. In the frequency region of the chaotic responses, the ultra-subharmonic resonance of 2/3 order is generated predominantly. Figure 5 shows the time histories, the frequency spectra, and the Poincaré projections of the representative chaotic response at the excitation frequency $\omega = 14.7$.

Figures 5(a) and (b) show the time histories of the deflection $\tilde{w}_1(0.5)$ and of the deflection $\tilde{w}_2(0.5)$ with the time progress, which is normalized by the excitation period τ_e. The time histories of the chaotic response include the phenomena of dynamic snap-through. The amplitudes of response of the horizontal beam are much larger than those of the vertical beam.

The Fourier spectra are shown in Figs. 5(c) and (d). The ordinate indicates the amplitude A of the spectrum scaled by decibel. The abscissa indicates the nondimensional Fourier frequency ω_{sp}. The solid circles on the abscissa indicate natural frequencies $\omega_i, (i = 1, 2, 3)$. In Fig. 5(c), the distinguished peaks of spectrum components are observed at the excitation frequency ω and the ultra-subharmonic frequency $(2/3)\omega$ predominantly. There are other peaks of spectrum corresponding to the subharmonic component $(1/2)\omega$ and the super-subharmonic component $(3/5)\omega$. In Fig. 5(d), the components of Fourier spectrum at the frequencies ω and $(2/3)\omega$ show the predominant peaks. The small peaks of spectrum are also observed neighboring to the natural frequencies ω_2 and ω_3.

The Poincaré projections of the chaotic response C(1;2/3) are shown in Figs. 5(e) and (f). The responses of the deflection $\tilde{w}_i(0.5), (i = 1, 2)$ and the velocity $\tilde{w}_{i,\omega\tau}(0.5), (i = 1, 2)$ are sampled at the phase delay $\theta = 0$ radian from the maximum amplitude of the excitation force. The projections show the typical chaotic attractors. The Poincaré projection of the vertical beam shows a fractal pattern more distinctly than that of the horizontal beam.

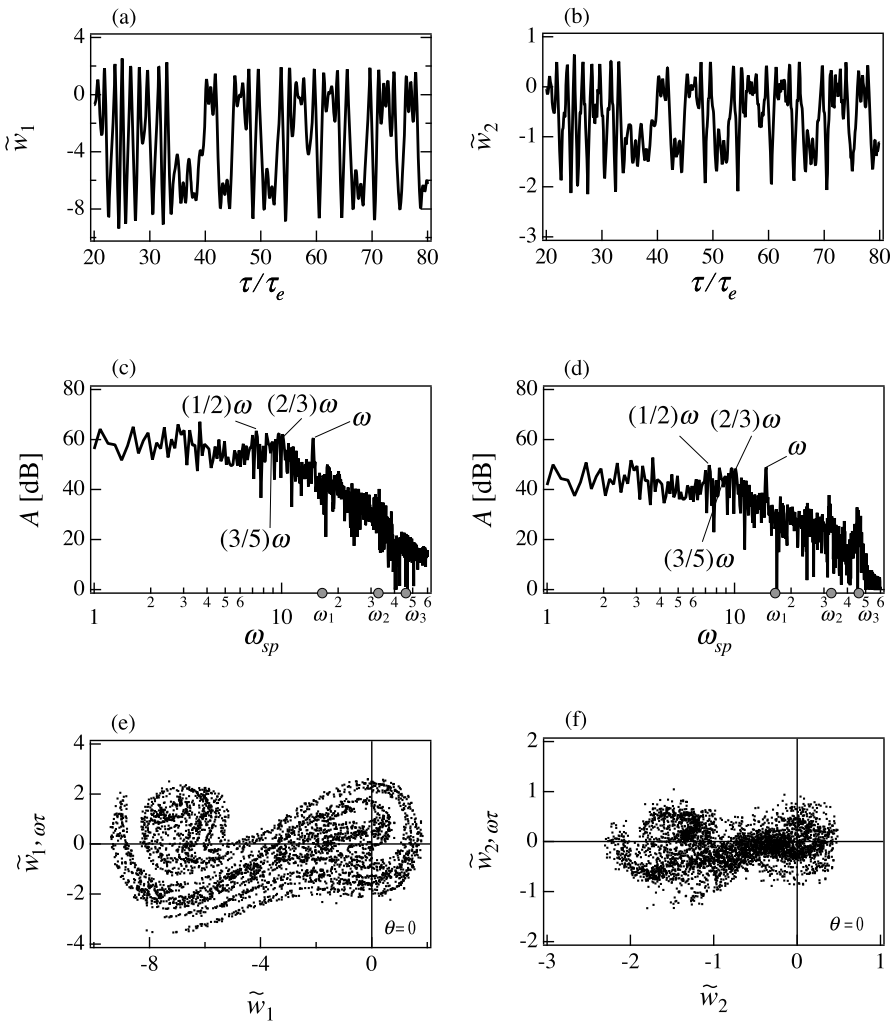

Fig. 5 Chaotic responses C(1;2/3) at the excitation frequency $\omega = 14.7$, (**a**) time history of the deflection $\tilde{w}_1(0.5)$; (**b**) time history of the deflection $\tilde{w}_2(0.5)$; (**c**) Fourier spectrum of the response $\tilde{w}_1(0.5)$; (**d**) Fourier spectrum of the response $\tilde{w}_2(0.5)$; (**e**) Poincaré projection between the deflection $\tilde{w}_1(0.5)$ and the velocity $\tilde{w}_{1,\omega\tau}(0.5)$; (**f**) Poincaré projection between the deflection $\tilde{w}_2(0.5)$ and the velocity $\tilde{w}_{2,\omega\tau}(0.5)$

5.4 Inspection of the chaotic responses

When a random-like response has more than one positive Lyapunov exponent, the response can be confirmed as the chaos. The maximum Lyapunov exponents of the chaotic responses C(1;2/3) are calculated by the Wolf's method. As shown in Fig. 6, Lyapunov exponents $\lambda_{\max}$ take the average value 1.9 within the frequency region from $\omega = 15.0$ to $\omega = 14.6$.

The Lyapunov dimension d_L of the chaotic response is calculated by changing the assumed number of vibration modes I_c. Figure 7 shows the Lyapunov dimension of the chaotic response C(1;2/3) at the excitation frequency $\omega = 14.7$. As the number of assumed mode I_c increases more than $I_c = 3$, the Lyapunov dimension d_L converges to $d_L = 3$. Therefore, three modes of vibration contribute predominantly to the chaotic response.

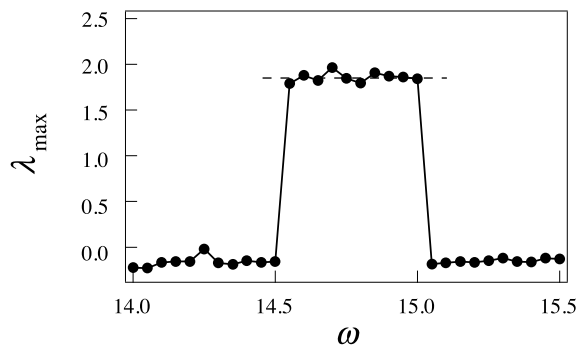

Fig. 6 Maximum Lyapunov exponents related to excitation frequency

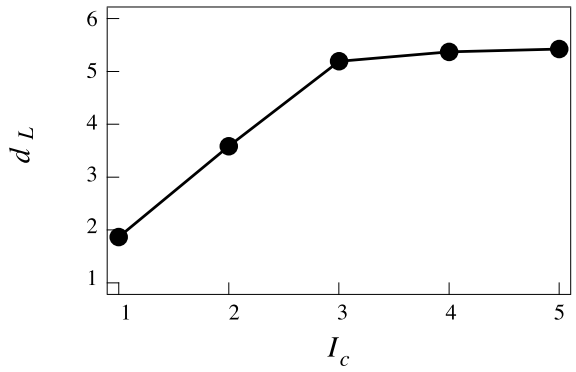

Fig. 7 Lyapunov dimension of the chaotic response C(1;2/3) at the excitation frequency $\omega = 14.7$

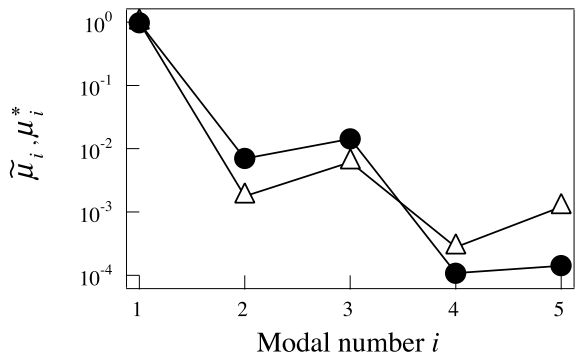

Fig. 9 Contribution ratio of vibration modes in the chaotic response C(1;2/3) at the excitation frequency $\omega = 14.7$, ●: the results of the POD with velocity $\tilde{w}_{i,\tau}$; △: simplified estimation with the value $\omega_i^2 p_i$

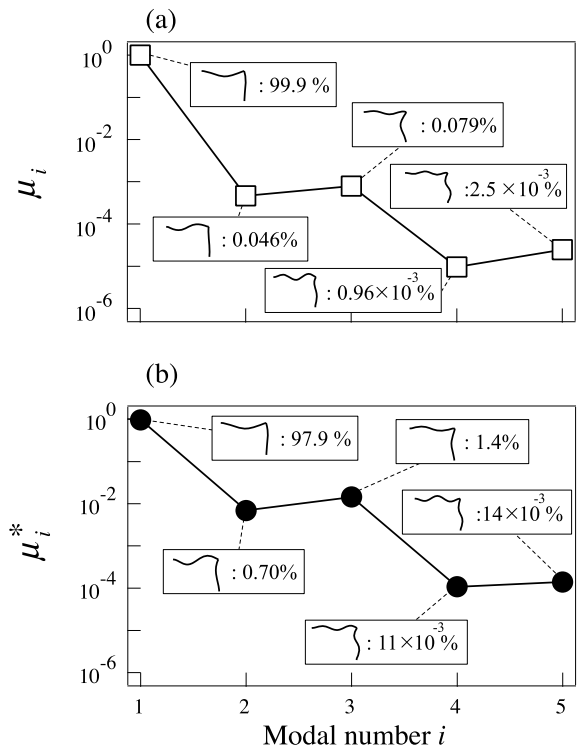

Fig. 8 Contribution ratio of each vibration mode in the chaotic response C(1;2/3) at the excitation frequency $\omega = 14.7$, (**a**) the results of the POD to deflection $\tilde{w}_i$; (**b**) the results of the POD to velocity $\tilde{w}_{i,\tau}$

To inspect the contribution of vibration modes to the chaotic responses C(1;2/3), the proper orthogonal decomposition (POD) is applied to the chaotic response. The chaotic response at the excitation frequency $\omega = 14.7$ is calculated under the assumed number of vibration modes $I_c = 5$. Figure 8 shows the contribution ratio to the modal number. Related modal patterns are also shown in the figure. Figure 8(a) shows the result of the POD applied to the responses of deflection. The ordinate in Fig. 8(a) indicates the contribution ratio μ_i which corresponds to the variance of deflection. Figure 8(b) is the result of the POD applied to the responses of velocity, where the ordinate indicates the contribution ratio μ_i^* which is related to the variance of velocity. The variance of velocity corresponds to kinetic energy of vibration modes.

In both of the figures, three modes of vibration contribute to the chaos dominantly. The three modes correspond to the lowest, second, and third modes of vibration. The lowest mode of vibration shows the largest contribution ratio in the modes. When kinetic energy of each vibration mode is evaluated with the variance of velocity, contribution of higher modes increases compared to the results of the variance of deflection.

To estimate kinetic energy of vibration modes with the variance of deflection, the value $\omega_i^2 p_i$ is calculated, where ω_i is natural frequency and p_i is eigenvalue derived from the variance of deflection written in Sect. 4.4. The value $\omega_i^2 p_i$ corresponds to kinetic energy of the vibration mode of ith order and is normalized as contribution ratio $\tilde{\mu}_i$. Figure 9 shows the contribution ratio $\tilde{\mu}_i$ as the simplified estimation compared with the contribution ratio μ_i^* calculated from the variance of velocity. The contribution ratio $\tilde{\mu}_i$ shows the similar order to the contribution ratio μ_i^* approximately. The same results are obtained at other excitation frequencies in the chaotic region.

6 Conclusions

Chaotic vibrations of a post-buckled L-shaped beam with an axial constraint have been analyzed theoretically. In the analysis, the governing equation including nonlinear boundary conditions was derived with the Lagrange's method of undetermined multiplier. The mode shape function was assumed to satisfy continuity conditions in a prebuckled state. Applying the modified Galerkin procedure to the governing equation, a set of nonlinear differential equations was reduced with a multiple degree-of-freedom system. Modes of vibration were calculated under the post-buckled configuration. Utilizing the modes of vibration, the standard form of nonlinear differential equations of the post-buckled L-shaped beam was obtained sequentially. Based on the set of nonlinear differential equation, chaotic responses were inspected in detail. The results are summarized as follows:

(1) Chaotic vibrations of the post-buckled L-shaped beam are generated with the ultra-subharmonic resonant response of 2/3 order corresponding to the lowest mode of vibration predominantly.
(2) The number of vibration modes contributing to the chaos is found to be three with the results of Lyapunov dimension and the proper orthogonal decomposition (POD).
(3) The contribution ratios in each mode are calculated to the kinetic energy in the POD. The contribution of the first mode of vibration to the chaotic response is dominant. The second and third modes contribute to the chaos with 1% and 2%, respectively.
(4) Contribution ratio is calculated with the response of deflection in the POD and natural frequencies. The results show the similar order to the results calculated with the response of velocity in the POD.

Appendix A

The coefficients c_{njk}, p_{1nj}, p_{2nj} and q_{nj} $(n = 1, 2; j, k = 1, \ldots, 5)$ are shown in the following Tables 3, 4 and 5.

Table 3 Coefficients c_{1jk} of the mode shape function $\zeta_{1j}(\xi_1)$

j	k				
	1	2	3	4	5
1	0.0000	0.0000	1.2129	−2.2129	1.0000
2	0.0000	0.0000	1.3168	−2.3167	1.0000
3	0.0000	0.0000	0.9899	−1.9899	1.0000
4	0.0000	0.0000	1.2217	−1.2217	1.0000
5	0.0000	0.0000	1.5322	−2.5321	1.0000

Table 4 Coefficients c_{2jk} of the mode shape function $\zeta_{2j}(\xi_2)$

j	k				
	1	2	3	4	5
1	0.0000	0.0000	0.1264	−0.1278	−0.0050
2	0.0000	0.0000	−0.6836	−1.1270	−0.4500
3	0.0000	0.0000	0.2662	−0.1861	−0.0500
4	0.0000	0.0000	−0.6439	−1.1005	−0.4500
5	0.0000	0.0000	2.1581	−4.1499	2.0000

Table 5 Coefficients p_{1nj}, p_{2nj} and q_{nj} $(n = 1, 2)$ of the mode shape function $\zeta_{nj}(\xi_n)$

j	p_{11j}	p_{12j}	q_{1j}	p_{21j}	p_{22j}	q_{2j}
1	0.000	0.000	0.000	0.000	0.000	0.000
2	0.870	−1.429	−0.038	0.000	0.000	0.000
3	1.013	−3.082	−0.007	0.563	−5.059	0.002
4	1.839	−0.820	−0.707	0.844	−2.042	0.001
5	2.335	−1.519	−0.848	0.986	−1.915	0.006

Appendix B

The coefficients in the nonlinear ordinary differential equation (23) are shown below.

$$\hat{B}_{ij} = J_{1ij}^{(0)} + l J_{2ij}^{(0)} + \gamma_e \zeta_{1i,\xi_1}(1)\zeta_{1j,\xi_1}(1), \tag{33}$$

$$\begin{aligned}\hat{C}_{ij} = {} & \frac{ku_s}{1+k}\left\{-\zeta_{1i}(1)\zeta_{1j,\xi_1}(1) + J_{1ij}^{(1)}\right\} \\ & + \left\{\zeta_{1i}(1)\zeta_{1j,\xi_1\xi_1\xi_1}(1) + J_{1ij}^{(1)}\right\} \\ & + \frac{1}{l^3}\left\{\zeta_{2i}(1)\zeta_{2j,\xi_2\xi_2\xi_2}(1) + J_{2ij}^{(1)}\right\} \\ & - \left\{\frac{ku_s}{1+k}\zeta_{1i,\xi_1}(1) - \zeta_{1i,\xi_1\xi_1\xi_1}(1)\right\}\zeta_{1j}(1)\end{aligned}$$

$$
\begin{aligned}
&- \frac{\Gamma_1^2 k l u_s}{1+k}\left\{\frac{k u_s}{1+k}\zeta_{1i,\xi_1}(1)\right.\\
&\left.- \zeta_{1i,\xi_1\xi_1\xi_1}(1)\right\}\zeta_{1j,\xi_1}(1)\\
&+ \frac{\Gamma_1^2 k l u_s}{1+k}\left\{\frac{k u_s}{1+k}\zeta_{1i,\xi_1}(1)\right.\\
&\left.- \zeta_{1i,\xi_1\xi_1\xi_1}(1)\right\}\zeta_{1j,\xi_1\xi_1\xi_1}(1)\\
&+ \frac{\Gamma_1^2 k^2 u_s^2}{(1+k)^2 l}\zeta_{2i,\xi_2}(1)\zeta_{1j,\xi_1}(1)\\
&- \frac{\Gamma_1^2 k u_s}{(1+k) l}\zeta_{2i,\xi_2}(1)\zeta_{1j,\xi_1\xi_1\xi_1}(1)\\
&+ \frac{\Gamma_1^2}{l^6}\zeta_{2i,\xi_2\xi_2\xi_2}(1)\zeta_{2j,\xi_2\xi_2\xi_2}(1)\\
&+ \frac{1}{l^3}\zeta_{2i,\xi_2\xi_2\xi_2}(1)\zeta_{2j}(1)\\
&+ \frac{\Gamma_1^2 k u_s}{(1+k) l}\left\{\frac{k u_s}{1+k}\zeta_{1i,\xi_1}(1)\right.\\
&\left.- \zeta_{1i,\xi_1\xi_1\xi_1}(1)\right\}\zeta_{2j,\xi_2}(1), \qquad (34)
\end{aligned}
$$

$$
\begin{aligned}
\hat{R}_{ij} = {} & \frac{\Gamma_1\beta_e}{l}\zeta_{2i}(1)\zeta_{2j,\xi_2}(1) + \frac{\Gamma_1\beta_e}{l}\zeta_{2i,\xi_2}(1)\zeta_{2j}(1)\\
&- \frac{\Gamma_1\beta_e}{l}J_{2ij}^{(1)} - \frac{\Gamma_1}{l^4}J_{2ij}^{(1)} + \frac{\Gamma_1}{l^4}K_{2ij1}, \qquad (35)
\end{aligned}
$$

$$
\begin{aligned}
\hat{D}_{ijk} = {} & \frac{\Gamma_1}{(1+k)l^3}\{-\zeta_{1i}(1)\zeta_{1j,\xi_1}(1)\\
&+ J_{1ij}^{(1)}\}\zeta_{2k,\xi_2\xi_2\xi_2}(1)\\
&+ \frac{\Gamma_1 k u_s}{(1+k)l}\{-\zeta_{2i}(1)\zeta_{2j,\xi_2}(1) + J_{2ij}^{(1)}\}\zeta_{1k,\xi_1}(1)\\
&- \frac{\Gamma_1}{l}\{-\zeta_{2i}(1)\zeta_{2j,\xi_2}(1) + J_{2ij}^{(1)}\}\zeta_{1k,\xi_1\xi_1\xi_1}(1)\\
&+ \frac{\Gamma_1}{2l}\left\{\frac{k u_s}{1+k}\zeta_{1i,\xi_1}(1) - \zeta_{1i,\xi_1\xi_1\xi_1}(1)\right\}J_{2jk}^{(1)}\\
&- \frac{\Gamma_1}{(1+k)l^3}\{\zeta_{2i,\xi_2\xi_2\xi_2}(1)\zeta_{1j,\xi_1}(1)\\
&+ \zeta_{1i,\xi_1}(1)\zeta_{2j,\xi_2\xi_2\xi_2}(1)\}\zeta_{1k}(1)\\
&- \frac{\Gamma_1 k u_s}{(1+k)l}\zeta_{2i,\xi_2}(1)\zeta_{1j,\xi_1}(1)\zeta_{2k}(1)\\
&+ \frac{\Gamma_1}{l}\zeta_{2i,\xi_2}(1)\zeta_{1j,\xi_1\xi_1\xi_1}(1)\zeta_{2k}(1)\\
&- \frac{\Gamma_1 k}{2(1+k)l^3}\zeta_{2i,\xi_2\xi_2\xi_2}(1)J_{1jk}^{(1)}\\
&+ \frac{\Gamma_1}{2l^3}\zeta_{2i,\xi_2\xi_2\xi_2}(1)J_{1jk}^{(1)}\\
&- \frac{\Gamma_1}{l}\left\{\frac{k u_s}{1+k}\zeta_{1i,\xi_1}(1)\right.\\
&\left.- \zeta_{1i,\xi_1\xi_1\xi_1}(1)\right\}\zeta_{2j,\xi_2}(1)\zeta_{2k}(1), \qquad (36)
\end{aligned}
$$

$$
\begin{aligned}
\hat{R}'_{ijk} = {} & \frac{\Gamma_1^2\beta_e}{(1+k)l}\{-\zeta_{1i}(1)\zeta_{1j,\xi_1}(1) + J_{1ij}^{(1)}\}\zeta_{2k,\xi_2}(1)\\
&+ \frac{\Gamma_1^2\beta_e}{2(1+k)l}\zeta_{2i,\xi_2}(1)J_{1jk}^{(1)}, \qquad (37)
\end{aligned}
$$

$$
\begin{aligned}
\hat{E}_{ijkl} = {} & \frac{k}{2(1+k)}\{-\zeta_{1i}(1)\zeta_{1j,\xi_1}(1) + J_{1ij}^{(1)}\}J_{1kl}^{(1)}\\
&+ \frac{\Gamma_1^2}{(1+k)l}\{-\zeta_{1i}(1)\zeta_{1j,\xi_1}(1)\\
&+ J_{1ij}^{(1)}\}\zeta_{1k,\xi_1\xi_1\xi_1}(1)\zeta_{2l,\xi_2}(1)\\
&+ \frac{\Gamma_1^2}{(1+k)l^4}\{-\zeta_{2i}(1)\zeta_{2j,\xi_2}(1)\\
&+ J_{2ij}^{(1)}\}\zeta_{2k,\xi_2\xi_2\xi_2}(1)\zeta_{1l,\xi_1}(1)\\
&+ \frac{\Gamma_1^2}{2(1+k)l^4}\{\zeta_{2i,\xi_2\xi_2\xi_2}(1)\zeta_{1j,\xi_1}(1)\\
&+ \zeta_{1i,\xi_1}(1)\zeta_{2j,\xi_2\xi_2\xi_2}(1)\}J_{2kl}^{(1)}\\
&- \frac{\Gamma_1^2}{(1+k)l^4}\{\zeta_{2i,\xi_2\xi_2\xi_2}(1)\zeta_{1j,\xi_1}(1)\\
&+ \zeta_{1i,\xi_1}(1)\zeta_{2j,\xi_2\xi_2\xi_2}(1)\}\zeta_{2k,\xi_2}(1)\zeta_{2l}(1)\\
&- \frac{\Gamma_1^2 u_s}{2(1+k)^2 l}\zeta_{2i,\xi_2}(1)\zeta_{1j,\xi_1}(1)J_{1kl}^{(1)}\\
&- \frac{\Gamma_1^2}{2(1+k)l}\zeta_{2i,\xi_2}(1)\zeta_{1j,\xi_1\xi_1\xi_1}(1)J_{1kl}^{(1)}\\
&- \frac{\Gamma_1^2}{l^4}\zeta_{2i,\xi_2}(1)\zeta_{2j}(1)\zeta_{2k,\xi_2\xi_2\xi_2}(1)\zeta_{1l,\xi_1}(1)\\
&+ \frac{\Gamma_1^2 k}{2(1+k)l}\left\{\frac{k}{1+k}u_s\zeta_{1i,\xi_1}(1)\right.
\end{aligned}
$$

$$- \zeta_{1i,\xi_1\xi_1\xi_1}(1)\Big\}\zeta_{2j,\xi_2}(1)J_{1kl}^{(1)}$$
$$- \frac{\Gamma_1^2}{2l}\left\{\frac{k}{1+k}u_s\zeta_{1i,\xi_1}(1)\right.$$
$$\left.- \zeta_{1i,\xi_1\xi_1\xi_1}(1)\right\}\zeta_{2j,\xi_2}(1)J_{1kl}^{(1)}, \tag{38}$$

$$\hat{F}_i = \frac{\Gamma_1 k u_s}{(1+k)l^3}\zeta_{2i,\xi_2\xi_2\xi_2}(1), \tag{39}$$

$$\hat{G}_i = I_{1i}$$
$$- \Gamma_1^2 l\beta_e\left\{\frac{ku_s}{1+k}\zeta_{1i,\xi_1}(1) - \zeta_{1i,\xi_1\xi_1\xi_1}(1)\right\}$$
$$+ \frac{\Gamma_1^2\beta_e}{l}\left\{\frac{ku_s}{1+k}\zeta_{2i,\xi_2}(1)\right\}$$
$$+ \frac{\Gamma_1^2}{l^2}\left\{\frac{ku_s}{1+k}\zeta_{1i,\xi_1}(1) - \zeta_{1i,\xi_1\xi_1\xi_1}(1)\right\}, \tag{40}$$

$$\hat{H}_i = \zeta_{1i}(l_s), \tag{41}$$

where the notations I_{ni}, $J_{nij}^{(m-1)}$, and K_{nij1} are defined as the following equations:

$$I_{ni} = \int_0^1 \zeta_{ni}^{(0)}\zeta_{nj}^{(0)}\,d\xi_n, \tag{42}$$

$$J_{nij}^{(m-1)} = \int_0^1 \zeta_{ni}^{(m-1)}\zeta_{nj}^{(m-1)}\,d\xi_n, \tag{43}$$

$$K_{nij1} = \int_0^1 \xi_n\zeta_{ni}^{(0)}\zeta_{nj}^{(0)}\,d\xi_n. \tag{44}$$

The notation $\zeta_{ni}^{(m)}$ represents mth order derivative of the mode shape function $\zeta_{ni}(\xi_n)$ with respect to the coordinate ξ_n.

References

1. Tseng, W.Y., Dugundji, J.: Nonlinear vibrations of a buckled beam under harmonic excitation. ASME J. Appl. Mech. **38**, 467–476 (1971)
2. Yamaki, N., Mori, A.: Non-linear vibrations of a clamped beam with initial deflection and initial axial displacement, part I: theory. J. Sound Vib. **71**(3), 333–346 (1980)
3. Yamaki, N., Otomo, K., Mori, A.: Non-linear vibrations of a clamped beam with initial deflection and initial axial displacement, part II: experiment. J. Sound Vib. **71**(3), 347–360 (1980)
4. Holmes, P.J.: A nonlinear oscillator with a strange attractor. Philos. Trans. R. Soc. Lond. A **292**, 419–448 (1979)
5. Moon, F.C., Holmes, P.J.: The magnetoelastic strange attractor. J. Sound Vib. **65**(2), 276–296 (1979)
6. Pezeshki, C., Dowell, E.H.: Generation and analysis of Lyapunov exponents for the buckled beam. Int. J. Non-Linear Mech. **24**(2), 79–97 (1989)
7. Nagai, K.: Nonlinear vibrations of a shallow arch under periodic lateral force (Theory). Trans. Jpn. Soc. Mech. Eng., C **51**(471), 2820–2827 (1985) (in Japanese)
8. Nagai, K.: Nonlinear vibrations of a shallow arch under periodic lateral force (2nd Report, Experiment). Trans. Jpn. Soc. Mech. Eng., C **52**(484), 3047–3054 (1986) (in Japanese)
9. Nagai, K.: Experimental study of chaotic vibration of a clamped beam subjected to periodic lateral forces. Trans. Jpn. Soc. Mech. Eng., C **56**(525), 1171–1177 (1990) (in Japanese)
10. Nagai, K., Yamaguchi, T.: Chaotic vibrations of a post-buckled beam carrying a concentrated mass (1st Report, Experiment). Trans. Jpn. Soc. Mech. Eng., C **60**(579), 3733–3740 (1994) (in Japanese)
11. Yamaguchi, T., Nagai, K.: Chaotic vibrations of a post-buckled beam carrying a concentrated mass (2nd Report, Theoretical analysis). Trans. Jpn. Soc. Mech. Eng., C **60**(579), 3741–3748 (1994) (in Japanese)
12. Yamaguchi, T., Nagai, K.: Chaotic oscillations of a shallow arch with variable cross section subjected to periodic excitation. Trans. Jpn. Soc. Mech. Eng., C **61**(583), 799–807 (1995) (in Japanese)
13. Maruyama, S., Nagai, K., Yamaguchi, T., Hoshi, K.: Contribution of multiple vibration modes to chaotic vibrations of a post-buckled beam with an axial elastic constraint. J. Syst. Des. Dyn. **2**(3), 738–749 (2008)
14. Yanagisawa, D., Nagai, K., Maruyama, S.: Chaotic vibrations of a clamped-supported beam with a concentrated mass subjected to static axial compression and periodic lateral acceleration. J. Syst. Des. Dyn. **2**(3), 762–773 (2008)
15. Nagai, K., Maruyama, S., Sakaimoto, K., Yamaguchi, T.: Experiments on chaotic vibrations of a post-buckled beam with an axial elastic constraint. J. Sound Vib. **304**, 541–555 (2007)
16. Wang, F., Bajaj, A.K.: Nonlinear normal modes in multimode models of an inertially coupled elastic structure. Nonlinear Dyn. **47**, 25–47 (2007)
17. Warminski, J., Cartmell, M.P., Bochenski, M., Ivanov, I.: Analytical and experimental investigations of an autoparametric beam structure. J. Sound Vib. **315**, 486–508 (2008)
18. Nayfeh, A.H., Zavodney, L.D.: Experimental observation of amplitude- and phase-modulated responses of two internally coupled oscillators to a harmonic excitation. ASME J. Appl. Mech. **55**, 706–710 (1988)
19. Nayfeh, A.H., Balachandran, B., Colbert, M.A., Nayfeh, M.A.: An experimental investigation of complicated responses of a two-degree-of-freedom structure. ASME J. Appl. Mech. **56**, 960–967 (1989)
20. Nagai, K., Arai, N., Nagaya, K., Takeda, S.: A flexural vibration analysis of a cantilevered beam carrying a concentrated mass by mode shape function approach. Trans. Jpn. Soc. Mech. Eng., C **55**(516), 1941–1947 (1989) (in Japanese)

21. Nagai, K., Nagaya, K., Takeda, S., Arai, N.: A free vibration of beams carrying a concentrated mass under distributed axial forces. Trans. Jpn. Soc. Mech. Eng., C **54**(497), 39–46 (1988) (in Japanese)
22. Wolf, A., Swift, J.B., Swinney, H.L., Vastano, J.A.: Determining Lyapunov exponents from a time series. Physica **16D**, 285–317 (1985)
23. Shimada, I., Nagashima, T.: A numerical approach to ergodic problem of dissipative dynamic systems. Prog. Theor. Phys. **61**, 1605–1616 (1979)
24. Kaplan, J., Yorke, J.: The Lyapunov dimension of strange attractors. J. Differ. Equ. **49**, 185–207 (1983)
25. Loève, M.M.: Probability Theory. Van Nostrand, Princeton (1955)
26. Feeny, B.F., Kappagantu, R.: On the physical interpretation of proper orthogonal modes in vibrations. J. Sound Vib. **211**(4), 607–616 (1998)
27. Yamaguchi, T., Nagai, K., Maruyama, S.: Identification of spatial modes in chaotic vibration involving dynamic snap-through using KL method. Trans. Jpn. Soc. Mech. Eng., C **69**(687), 2937–2942 (2003) (in Japanese)
28. Azeez, M.F.A., Vakakis, A.F.: Proper orthogonal decomposition of a class of vibroimpact oscillations. J. Sound Vib. **240**, 859–889 (2001)